Eur. Phys. J. Appl. Phys. (2016) 74: 24611
DOI: 10.1051/epjap/2015150383

THE EUROPEAN PHYSICAL JOURNAL APPLIED PHYSICS

Regular Article

Optical properties of undoped and tin-doped nanostructured In_2O_3 thin films deposited by spray pyrolysis*

Nabil Fellahi[a], Mohammed Addou, Amina Kachouane, Mohamed El Jouad, and Zouhair Sofiani

Optoelectronics and Physical Chemistry of Materials Laboratory, Unit Research Associated CNRST-URAC, Ibn Tofail University, Faculty of Sciences, BP 133, Kénitra 14000, Morocco

Received: 23 July 2015 / Received in final form: 17 November 2015 / Accepted: 16 December 2015
Published online: 3 May 2016 –

Abstract. Tin-doped indium oxide (In_2O_3:Sn) thin films in different concentrations (Sn = 0, 3, 5, 8 at.%) were deposited by reactive chemical pulverisation spray pyrolysis on heated glass substrates at 500 °C. The effect of the tin dopant on the nonlinear optical properties was investigated using X-ray diffraction, transmission, electrical resistivity and third harmonic generation (THG). All films were polycrystalline, and crystallised in a cubic structure with a preferential orientation along the (4 0 0) direction. The Sn (5 at.%) doped In_2O_3 thin films exhibited a lower resistivity of 3×10^{-4} Ω cm, and higher transmission in the visible region of about 94%. Optical parameters, such as the extinction coefficient (k), refractive index (n) and energy band gap (E_g), were also studied to show the composition-dependence of tin-doped indium oxide films. The nonlinear properties of the In_2O_3:Sn thin films have been found to be influenced by doping concentration, and the best value of $\chi^{(3)} = 3 \times 10^{-11}$ (esu) was found for the 5 at.% doped sample.

1 Introduction

High optical transparency in the visible region (over 80%), low electrical resistivity (less than 10^{-3} Ω cm) and high infrared reflectivity make tin-doped indium oxides (In_2O_3:Sn, ITO) good candidates for many potential applications, such as liquid crystal displays, solar cells and organic electroluminescence diodes [1–3]. Different techniques have been used for growth of thin films: high-intensity pulsed ion beam (HIPIB) [4], horizontal in-line sputtering system [5], co-precipitation [6], thermal co-evaporation [7], dip coating [8] and electron beam evaporation [9,10]. Here we have prepared ITO films using the spray pyrolysis technique, which can be distinguished from other techniques by its simplicity, low cost and process yield. This is basically a chemical deposition technique, where the most important deposition parameters are: the precursors, the solution concentration, the deposition temperature and the spray rate. The effects on the structural, morphological, electrical and linear optical properties induced by tin-doped indium oxide have been extensively studied [9,11,12]. However, to our knowledge, a description of the nonlinear optical properties has not been reported in the literature. In this paper, we report on the efficient third-harmonic generation (THG) in thin films of In_2O_3 and In_2O_3:Sn, prepared by spray pyrolysis, leading to direct generation of UV light from a Q-switched mode-locked Nd:YAG (λ = 1064 nm) laser (model: quantum elite).

Among the methods used for the investigation of the nonlinear optical parameters of materials are optical phase conjugation [13], degenerate four-wave mixing (DFWM) [14], nonlinear interferometry [15], the Z-scan technique [16] and third harmonic generation (THG) [17–19]. Because of the high frequencies involved, THG can probe purely coherent electronic nonlinearity. This technique also permits exploration of the absorption edge of the material without damaging the sample using the strong fundamental beam. One advantage of the THG technique is that the TH response accounts only for the ultrafast electronic response, so that vibrational, orientational and thermal effects, which may contribute to the overall nonlinear response of the material, are excluded.

2 Experimental details

Indium oxide films were prepared from a solution of indium chloride ($InCl_3$) dissolved in deionised water and transported in tubes using a pump flow meter to regulate the spray rate of the solution, which is sprayed in fine droplets using air as a carrier gas. Tin chloride ($SnCl_2$: $2H_2O$) was used as a doping agent, where the [Sn]/[In] ratio varied between 0 and 8 at.%. This solution was sprayed onto clean glass substrates with a size of (25 mm × 25 mm × 1 mm) heated by a ceramic heater.

[a] e-mail: fellahinabil@yahoo.fr

* Contribution to the topical issue "Materials for Energy Harvesting, Conversion and Storage (ICOME 2015) – Elected submissions", edited by Jean-Michel Nunzi, Rachid Bennacer and Mohammed El Ganaoui

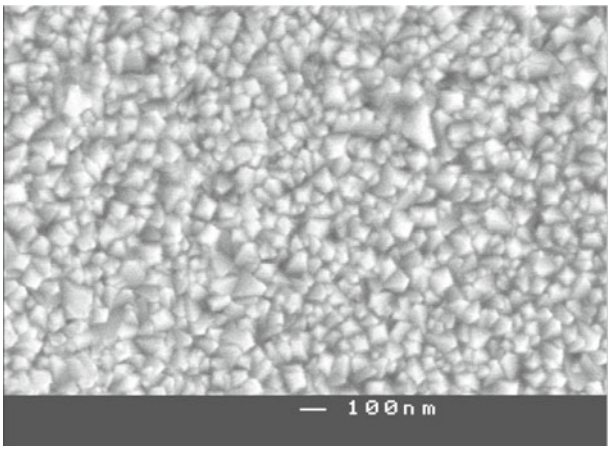

Fig. 1. SEM images of In_2O_3:Sn (5 at.%) prepared at 500 °C.

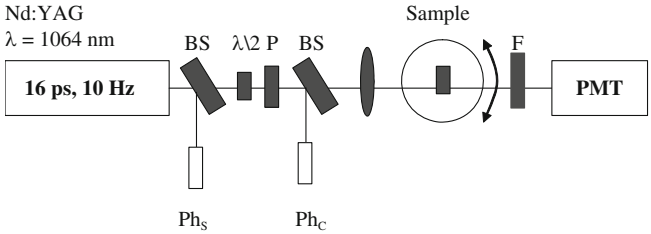

Fig. 2. THG experimental setup, Ph_S: synchronisation photodiode, Ph_C: control photodiode, $\lambda/2$: half wave plate, BS: beam splitter, P: polariser, F: transmitting filter at 355 nm, PMT: photomultiplier tube.

The indium chloride concentration, the solution flow rate and the substrate temperature were optimised after several depositions and were fixed at 0.05 M, 5 mL/min and 500 °C, respectively. The nozzle was directed towards the substrate (distance nozzle-substrate = 40 cm). The schematic set-up for the preparation of pyrolytically spray deposited films was described in reference [20].

The average thickness of the deposited films (∼200 nm) was measured using a Tencor Alpha-step profilometer. The films reported in this study show a smooth and fully covered surface with uniform distribution of the grains (see Fig. 1). The structural characterisations are performed using X-ray diffraction (XRD) with Cu Kα radiation wavelength (λ = 1.5418 Å). The optical transmission measurements were performed with a Shimadzu 3101 PC UV-Vis-NIR spectrophotometer. The electrical resistivity was measured at room temperature by the Van Der Paw method.

Third harmonic generation (THG) measurements (see Fig. 2) were performed using a Q-switched mode-locked Nd:YAG (λ = 1064 nm) laser (model: quantum elite) as the pump beam. It offers 1.62 mJ/pulse (pulse duration 15 ps) at 10 Hz. The fundamental beam energy was controlled with a polariser and a half wave plate then focussed on the sample through a lens with a focal length of 25 cm. The beam diameter was 0.65 mm and the applied power density was 2 GW/cm^2. The sample was mounted on a rotational step motor. A selective filter (at 355 nm) is used to absorb the pump beam letting only the generated one bes collected in a tube photomultiplier (PMT). We also used density filters to reduce the generated intensity by the nonlinear medium. The third harmonic signal was detected by PMT (model: Hamamatsu), which was integrated with a boxcar and processed by a computer. A portion of the input beam was picked off and measured by a fast photo-diode to monitor the input energy. Finally we got the so-called Maker-fringes, which were generated by rotating the sample through the range from ±50 to the normal.

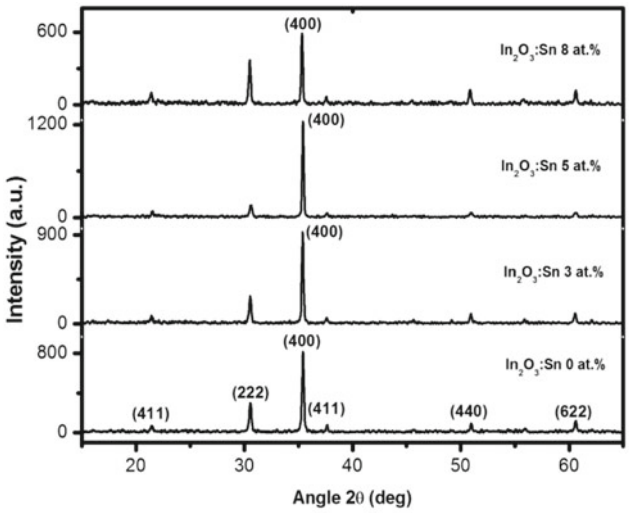

Fig. 3. XRD patterns of the ITO films with different Sn doping concentrations.

3 Results and discussion

3.1 Structural properties

X-ray diffraction spectra recorded for Sn-doped In_2O_3 films for different Sn concentrations deposited at a substrate temperature of 500 °C using the spray pyrolysis technique are shown in Figure 3. The analysis of the crystalline structure reveals that all the films are polycrystalline and crystallise in a cubic structure. For all the samples, the peak intensity of the (400) plane was predominant among the other reflection planes, indicating the preferential orientation of the ITO film. The intensity ratio of (400) to the total intensities of main orientations like (622), (440), (400), (222) and (411), using the formula:

$$T_{(400)} = \frac{I_{(400)}}{I_{(622)} + I_{(440)} + I_{(400)} + I_{(222)} + I_{(411)}}, \quad (1)$$

is used to evaluate the doping effect on the film texture (Tab. 1). The value of $T_{(400)}$ should be unity for a perfectly (400) oriented film. From Table 1, the ratio $T_{(400)}$ increases with increasing Sn doping concentrations, peaking at 5 at.% Sn with a clear predominance of the (400) peak. This means that the compactness of the films is

Table 1. Values of band gap, average visible transmittance (AVT), intensity ratio $T_{(400)}$ and grain size of undoped and Sn-doped In_2O_3 thin films.

Samples	Band gap (eV)	AVT (%) (400–900) (nm)	$T_{(400)}$	Grain size D (nm)
In_2O_3	3.49	84	0.54	38
In_2O_3:Sn 3%	3.54	85.4	0.59	43
In_2O_3:Sn 5%	3.91	93.8	0.74	44
In_2O_3:Sn 8%	3.70	82.5	0.43	41

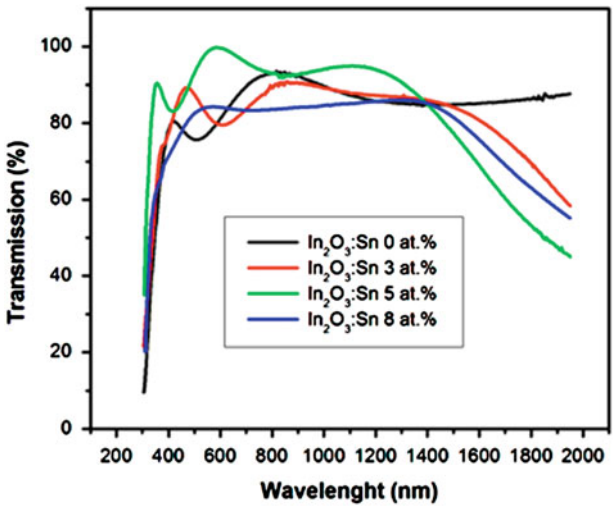

Fig. 4. Optical transmittance spectra of ITO films as a function of Sn-doping levels.

improved and the number of intergrain voids and defects reduced [21], which is consistent with an improvement in crystallinity. Note also that no characteristic peaks of impurity or dopant phases have been observed.

The crystalline sizes D were calculated from the (4 0 0) diffraction peaks using Debye-Scherrer's formula [22], and are listed in Table 1. The mean crystal diameter was $D \approx$ 44 nm for the sample deposited at 5 at.% Sn, which has a larger value than all other samples. We concluded that the films, which present large grain size, exhibit good crystallinity.

3.2 Optical properties

Figure 4 shows the optical transmittance spectra of the ITO films as a function of Sn-doping levels in wavelengths ranging from 250 to 2000 nm. It can be observed that the optical transmittance of the films was affected by the doping concentration. All of the films exhibit a high value of average optical transmittance (greater than 82%) in the visible region, and a maximum average visible transmittance (AVT) of ∼94% was obtained for the Sn doping (5 at.%) (AVT is shown in Tab. 1). This could be due to less pronounced scattering effects, structural homogeneity and better crystallinity. In contrast, the observed reflectance in the infrared region is due to a plasma effect

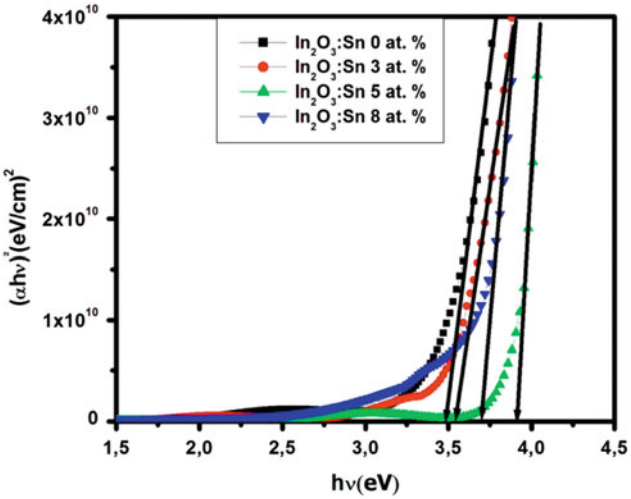

Fig. 5. Variation of optical band gap energy of ITO films with different Sn doping concentrations.

resulting from the high concentration of free electrons in our thin films. Furthermore, the absorption edge shifts towards shorter wavelengths, suggesting a widening of the energy band-gap with increasing Sn-concentration.

The optical band gap of the films is determined by applying the Tauc model in the high absorption region:

$$\alpha h\nu = A\left(h\nu - E_{\mathrm{g}}\right)^{n}, \tag{2}$$

where α is the absorption coefficient, $h\nu$ is the photon energy, E_{g} is the optical band gap and A is a constant. For $n = 1/2$ the transition data provide the best linear curve in the band edge region, implying that the transition is direct in nature. The band gap of the films has been calculated using the Tauc plot of $(\alpha h\nu)^2$ versus $h\nu$ (shown in Fig. 5) and by extrapolating the linear portion of the absorption edge to find the intercept with the energy axis (at $\alpha h\nu = 0$). The estimated values of E_{g} are given in Table 1. The value of 3.49 eV obtained for the undoped films is found to increase with increasing Sn doping and appeared to reach a maximum of 3.91 eV at 5 at.% Sn. For ITO thin films, a wide range of E_{g} values from 3.5 to 4.3 eV have been reported in the literature [23]. The increase in band gap has been related to the increase in carrier concentration of the films and explained by the Burstein-Moss effect [24].

Figures 6a and 6b show the plot of refractive index and extinction coefficient as a function of wavelength for different concentrations of Sn-doped In_2O_3 films. The transmission performance was related to the refractive index and the extinction coefficient. The refractive index (n) was evaluated from the measured transmittance versus wavelength [25]:

$$n = \left[M + \left(M^2 - n_{\mathrm{s}}^2\right)^{\frac{1}{2}}\right]^{\frac{1}{2}}$$
$$M = 2n_{\mathrm{s}}\frac{T_{\mathrm{M}} - T_{\mathrm{m}}}{T_{\mathrm{m}}T_{\mathrm{M}}} + \frac{n_{\mathrm{s}}^2 + 1}{2}, \tag{3}$$

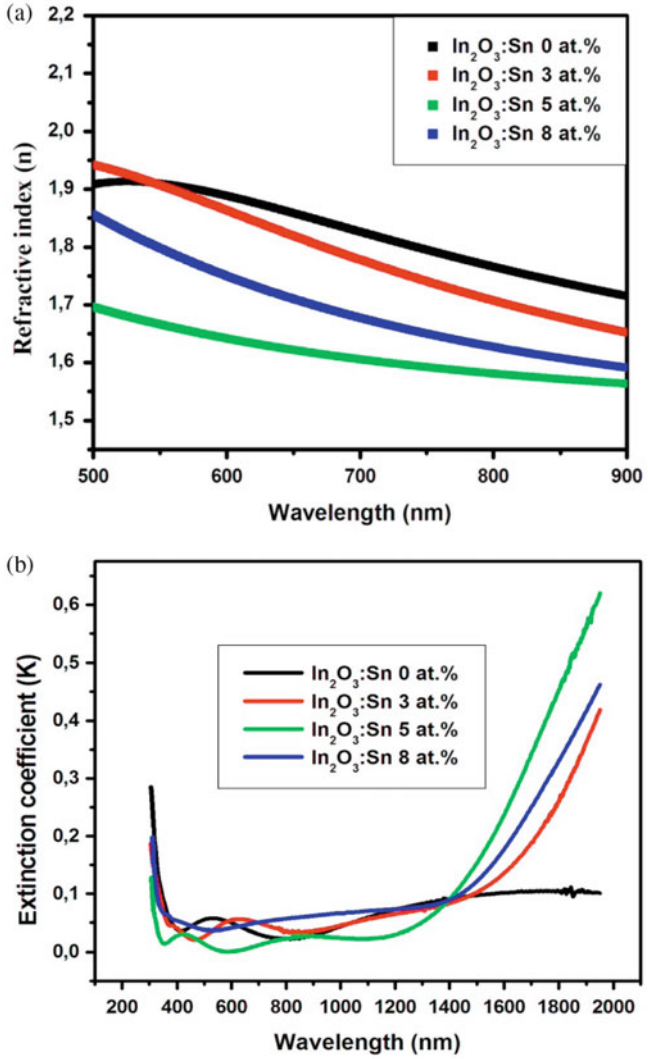

Fig. 6. Wavelength dependence of (a) the refractive index and (b) the extinction coefficient of ITO films with different Sn doping concentrations.

where n_s is the refractive index of the substrate, T_m and T_M are the experimental values of transmission at minimum or maximum points of a particular fringe.

The refractive index was found to decrease with wavelength, i.e., $dn/d\lambda < 0$; this behaviour was consistent with what one would expect from the Kramers-Kronig analysis [26]. It was observed that the refractive indices of the Sn-doped In_2O_3 thin films were smaller than those of the pure In_2O_3 film in the measured wavelength range. The decrease in refractive index with the increase of Sn-doping level was attributed to the increase of the carrier concentrations, which is consistent with other authors' results [27,28].

The extinction coefficient (k) was directly calculated from the absorption coefficient (α) by using the relation [29]:

$$k = \frac{\alpha\lambda}{4\pi}. \quad (4)$$

Table 2. Values of the $\chi^{(3)}$ and electrical resistivity for undoped and Sn doped In_2O_3 thin films.

Samples	ρ (Ω cm)	$(\chi^{(3)} \pm 0.1) \times 10^{-11}$ (esu)
In_2O_3	8×10^{-1}	1.44
In_2O_3:Sn 3%	1.2×10^{-3}	2.35
In_2O_3:Sn 5%	3×10^{-4}	3.00
In_2O_3:Sn 8%	6×10^{-4}	2.65

As can be seen in Figure 6b, the low value of the extinction coefficient in the visible region indicates the low roughness of the prepared samples. In addition, k for the sample In_2O_3:Sn (5 at.%) is lower than that of other samples due to an improvement in the crystallinity. The high extinction coefficient in the near infrared region may be due to the interaction of light with the free carriers at the plasma wavelength for the present films.

3.3 Electrical properties

The variation of the electrical resistivity of the ITO films deposited at various Sn-doping levels is given in Table 2. The resistivity significantly decreased with an increase in Sn doping to reach a minimum of $\rho = 3 \times 10^{-4}$ Ω cm at 5 at.% Sn. Afterwards, the resistivity increased slowly with the Sn concentration, reaching a value of $\rho = 6 \times 10^{-4}$ Ω cm at 8 at.% Sn. Similar behaviour was observed elsewhere [30,31]. When the concentration of Sn atoms is increased, they probably do not occupy proper lattice sites in the In_2O_3 crystallites because of their solubility limit in In_2O_3. As shown in the literature [32], the maximum solubility of Sn-atoms in the In_2O_3 lattice is reached at approximately 5 at.%. So for an atomic concentration of Sn lower than 5 at.%, the Sn^{4+} ions substitute In^{3+} ions in the cation sublattice. As Sn^{4+} replace In^{3+}, Sn atoms act as n-type donors, and the resistivity decreases with the Sn concentration. As the ionic radius of Sn is smaller than that of In, the excess Sn atoms (>5 at.%) may occupy interstitial positions, which act as charged trapping centres for the electrons [33], and thus the resistivity increases. The foregoing discussion leads to the conclusion that the films which present low electrical resistivity, low refractive index and a wide optical band gap have a higher free carrier concentration.

3.4 THG measurements

THG is a third order nonlinear optical process, in which the fundamental beam at wavelength λ interacts with a nonlinear medium and generates a beam at the wavelength $\lambda/3$ [17,18]. The analysis of experimental results was carried out on the basis of the Maker-fringes technique [34] so the third order nonlinear optical susceptibility $\chi^{(3)}$ of the samples was calculated. The $\chi^{(3)}$ can be expressed as [19]:

$$\chi^{(3)} = \chi_s^{(3)} \left(\frac{\pi}{2}\right) \left(\frac{L_{c,s}}{l}\right) \left(\frac{I_{3\omega}}{I_{3\omega,s}}\right)^{\frac{1}{2}}, \quad (5)$$

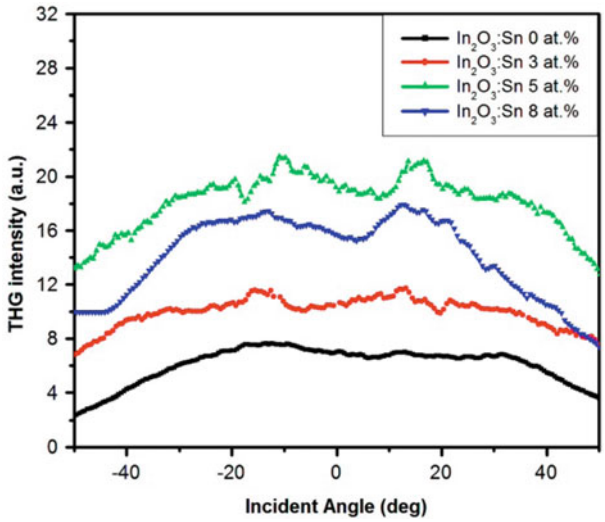

Fig. 7. Normalised third harmonic response of undoped and Sn-doped In_2O_3 thin films.

where $I_{3\omega}$ is the intensity of the THG signal, l is the film thickness, the suffix s refers to the reference material, as silica, $L_{c,s}$ is the coherence length of the microscope slide which is around 17.69 μm and $\chi_s^{(3)} = 4.38 \times 10^{-14}$ (esu) is the nonlinear optical susceptibility of the silica.

The aim of our investigation is to find an optimal tin content to obtain a higher value of $\chi^{(3)}$ than those already reported [30]. The experimental result of THG intensity as a function of incident angle is presented in Figure 7. It can be observed that the 5 at.% doped samples adopt the symmetric fringes with higher intensity. The calculated values for all the samples using equation (5) are given in Table 2. From these results, it can be seen that the incorporation of the tin improves the nonlinear response. The doped thin films showed higher values than the undoped layers. It is known that the third harmonic generation (THG) method allows determination of the purely electronic contribution to third order nonlinear optical susceptibility [35]. Doping of In_2O_3 with Sn increases the carrier concentration and thus decreases the electrical resistivity. When the electrical resistivity decreases, the values of the nonlinear optical properties increase [30]. The highest susceptibility value $\chi^{(3)} = 3 \times 10^{-11}$ (esu) is found for the In_2O_3:Sn (5 at.%) thin film. This seems to be due to its lower electrical resistivity of 3×10^{-4} Ω cm compared to all of the other samples (see Tab. 2).

4 Conclusions

In summary, doping of In_2O_3 with Sn has an important influence on the properties of nanocrystalline ITO thin films, prepared by the spray pyrolysis method. The films doped with 5 at.% Sn exhibit good crystallinity, high transmission (about 94%) in the visible region, low refractive index and very low electrical resistivity of 3×10^{-4} Ω cm. The nonlinear optical properties have been studied through third harmonic generation. We have found that doping by tin improves the nonlinear response. To get a high third harmonic generation we need a low electrical resistivity in thin films. The best value of $\chi^{(3)} = 3 \times 10^{-11}$ (esu) was found for the In_2O_3:Sn (5 at.%) samples at 500 °C.

This work is supported by Hassan II Academy of Science and Technology.

References

1. N. Huby, L. Hirsch, G. Wantz, L. Vignau, A.S. Barriere, J.P. Parneix, L. Aubouy, P. Gerbier, J. Appl. Phys. **99**, 084907 (2006)
2. H. Hong, S. Kim, D. Kim, T. Lee, J. Song, J.H. Cho, C. Sone, Y. Park, T. Seong, Appl. Phys. Lett. **88**, 103505 (2006)
3. C. Di, G. Yu, Y. Liu, X. Xu, Y. Song, D. Zhu, Appl. Phys. Lett. **89**, 033502 (2006)
4. W. Chengyu, L. Yongxing, X. Yuanliang, M. Tengcai, P.W. Wang, J. Non-Cryst. Solids **353**, 2244 (2007)
5. J. Liu, H. Wang, Y.R. Yang, Surf. Coat. Technol. **267**, 45 (2015)
6. H.-Y. Lai, T.-H. Chen, C.-H. Chen, Mater. Lett. **65**, 3336 (2011)
7. K.S. Park, C.G. Lee, H.S. Hong, I.S. Lee, S.J. Kwon, J.G. Park, Ceram. Int. **40**, 11727 (2014)
8. Y. Seki, Y. Sawada, M.H. Wang, H. Lei, Y. Hoshi, T. Uchida, Ceram. Int. **38S**, S613 (2012)
9. V. Senthilkumar, P. Vickraman, M. Jayachandran, C. Sanjeeviraja, Vacuum **84**, 864 (2010)
10. A.S.A.C. Diniz, Renew. Energy **36**, 1153e (2011)
11. N. Oka, Y. Kawase, Y. Shigesato, Thin Solid Films **520**, 4101 (2012)
12. C.-C. Ting, W.-L. Cheng, G.-C. Lin, Thin Solid Films **519**, 4286 (2011)
13. T. Tokizaki, A. Nakamura, S. Kaneko, K. Uchida, S. Omi, H. Tanji, Y. Asahara, Appl. Phys. Lett. **65**, 941 (1994)
14. H.B. Liao, R.F. Xiao, J.S. Fu, H. Wang, K.S. Wong, G.K.L. Wong, Opt. Lett. **23**, 388 (1998)
15. M.J. Morgan, C.Y. She, R.L. Carman, IEEE J. Quantum Electron. **11**, 259 (1975)
16. M. Sheik-Bahae, A.A. Said, T.-H. Wei, D.J. Hagan, E.W. Van Stryland, IEEE J. Quantum Electron. **26**, 760 (1990)
17. F. Kajzar, J. Messier, Phys. Rev. A **32**, 2352 (1987)
18. F. Kajzar, J. Messier, C. Rosilio, J. Appl. Phys. **60**, 3040 (1986)
19. X.H. Wang, D.P. West, N.B. McKeown, T.A. King, J. Opt. Soc. Am. B **15**, 1895 (1998)
20. M. Addou, A. Moumin, B. Elidrissi, M. Regragui, A. Bougrine, A. Kachouane, C. Monty, J. Chem. Phys. **96**, 232 (1999)
21. B. Zhang, X. Dong, X. Xu, J. Wu, Scripta Materialia **58**, 203 (2008)
22. L.D. Kadam, P.S. Patil, Mater. Chem. Phys. **68**, 225 (2001)
23. D. Raoufi, A. Kiasatpour, H.R. Fallah, A.S.H. Rosatian, Appl. Surf. Sci. **253**, 9085 (2007)
24. M. Girtan, G.I. Rusu, G.G. Rusu, S. Gurlui, Appl. Surf. Sci. **492**, 162 (2000)
25. R. Swanepoel, J. Phys. E: Sci. Instrum. **16**, 1214 (1983)

26. B. Sasi, P.K. Gopchandran Manoj, P. Koshy, P.P. Rao, V.K. Vaidyan, Vacuum **68**, 149 (2003)
27. H. Fujiwara, M. Kondo, Phys. Rev. B **71**, 075109 (2005)
28. L. Lin, F. Lai, Y. Qu, R. Gai, Z. Huang, Mat. Sci. Eng. B **138**, 166 (2007)
29. A.M. Elkorashy, Semicond. Sci. Technol. **4**, 382 (1989)
30. N. Fellahi, M. Addou, Z. Sofiani, M. El Jouad, K. Bahedi, S. Bayoud, M. Haouti, B. Sahraoui, J.C. Bernede, J. Optoelectron. Adv. Mater. **12**, 1087 (2010)
31. S. Parthiban, E. Elangovan, K. Ramamurthi, R. Martins, E. Fortunato, Sol. Energy Mater. Sol. Cells **94**, 406 (2010)
32. G. Frank, H. Kostlin, A. Rabenau, Phys. Status Solid A **52**, 231 (1979)
33. I. Hamberg, C.G. Granqvist, J. Appl. Phys. **60**, R123 (1986)
34. P.D. Maker, R.W. Terhune, M. Niseno, C.M. Savage, Phys. Rev. Lett. **8**, 21 (1962)
35. B. Derkowska, Z. Essaidi, B. Sahraoui, A. Marasek, F. Firszt, M. Kujawa, Opt. Materials **31**, 518 (2009)